

The airborne mass spectrometer AIMS – Part 1

S. Kaufmann et al.

This discussion paper is/has been under review for the journal Atmospheric Measurement Techniques (AMT). Please refer to the corresponding final paper in AMT if available.

The airborne mass spectrometer AIMS – Part 1: AIMS-H₂O for UTLS water vapor measurements

S. Kaufmann¹, C. Voigt^{1,2}, T. Jurkat¹, T. Thornberry^{3,4}, D. W. Fahey^{3,4}, R.-S. Gao³, R. Schlage¹, D. Schäuble⁵, and M. Zöger⁶

¹Deutsches Zentrum für Luft- und Raumfahrt, Institut für Physik der Atmosphäre, Oberpfaffenhofen, Germany

²Johannes Gutenberg-Universität, Institut für Physik der Atmosphäre, Mainz, Germany

³NOAA Earth System Research Laboratory, Chemical Sciences Division, Boulder, Colorado, USA

⁴University of Colorado, CIRES, Boulder, Colorado, USA

⁵Institute for Advanced Sustainability Studies, Potsdam, Germany

⁶Deutsches Zentrum für Luft- und Raumfahrt, Flight Experiments, Oberpfaffenhofen, Germany

Received: 27 November 2015 – Accepted: 27 November 2015 – Published: 21 December 2015

Correspondence to: S. Kaufmann (stefan.kaufmann@dlr.de)

Published by Copernicus Publications on behalf of the European Geosciences Union.

Title Page

Abstract

Introduction

Conclusions

References

Tables

Figures



Back

Close

Full Screen / Esc

Printer-friendly Version

Interactive Discussion



Abstract

In the upper troposphere and lower stratosphere (UTLS), the accurate quantification of low water vapor concentrations has presented a significant measurement challenge. The instrumental uncertainties are passed on to estimates of H₂O transport, cloud formation and the H₂O role in the UTLS energy budget and resulting effects on surface temperatures. To address the uncertainty in UTLS H₂O determination, the airborne mass spectrometer AIMS-H₂O, with in-flight calibration, has been developed for fast and accurate airborne water vapor measurements.

We present the new setup to measure water vapor by direct ionization of ambient air. Air is sampled via a backward facing inlet that includes a bypass flow to assure short residence times (< 0.2 s) in the inlet line, which allows the instrument to achieve a time resolution of ~ 4 Hz. From the main inlet flow, a smaller flow is extracted into the novel pressure-controlled gas discharge ion source of the mass spectrometer. The air is directed through the gas discharge region where water molecules react to form hydronium ion clusters, H₃O⁺(H₂O)_n (*n* = 0, 1, 2), in a complex reaction scheme similar to the reactions in the D-region of the ionosphere. These ions are counted to quantify the ambient water vapor mixing ratio. The instrument is calibrated during flight using a new calibration source based on the catalytic reaction of H₂ and O₂ on a Pt surface to generate a calibration standard with well defined and stable H₂O mixing ratios. In order to increase data quality over a range of mixing ratios, two data evaluation methods are presented for lower and higher H₂O mixing ratios respectively, using either only the H₃O⁺(H₂O) ions or the ratio of all water vapor dependent ions to the total ion current. Altogether, a range of water vapor mixing ratios from 1 to 500 ppmv (mole ratio, 10⁻⁶ mol mol⁻¹) can be covered with an accuracy between 7 and 15 %. AIMS-H₂O was deployed on two DLR research aircraft, the Falcon during CONCERT (Contrail and Cirrus Experiment) in 2011, and HALO during ML-CIRRUS (Mid-Latitude Cirrus) in 2014. The comparison of AIMS-H₂O with the SHARC tunable diode laser hygrometer

The airborne mass spectrometer AIMS – Part 1

S. Kaufmann et al.

Title Page

Abstract

Introduction

Conclusions

References

Tables

Figures



Back

Close

Full Screen / Esc

Printer-friendly Version

Interactive Discussion



The airborne mass spectrometer AIMS – Part 1

S. Kaufmann et al.

Title Page

Abstract

Introduction

Conclusions

References

Tables

Figures



Back

Close

Full Screen / Esc

Printer-friendly Version

Interactive Discussion



during ML-CIRRUS in 2014. Its twin configuration, AIMS-TG for trace gas observations, has also been operated on the DLR Falcon during CONCERT (Voigt et al., 2014) and on HALO during TACTS/ESMVal (Transport and Composition in the UT/LMS/Earth System Model Validation) in 2012 (Jurkat et al., 2014). In this work, we first describe the mechanical and electrical setup of AIMS-H₂O with a special emphasis on the novel gas discharge ion source designed for the direct ionization of ambient water vapor. Second, the in-flight calibration setup and performance to assure accurate and reliable airborne measurements is presented. After a discussion of data reduction methods used to quantify ambient H₂O mixing ratios, we derive the instrumental uncertainties and present the first airborne measurements on HALO during ML-CIRRUS including a comparison with the in situ tunable diode laser hygrometer SHARC.

2 Setup of the mass spectrometer

AIMS consists of a linear quadrupole mass spectrometer (Huey et al., 1995) which was designed and built by THS instruments at the Georgia Institute of Technology (Greg Huey, Atlanta, USA). It is integrated in one HALO standard rack plus an external plate where the bypass pump is mounted (behind the rack in Fig. 1). The instrument is connected to a heated HALO Trace Gas Inlet (TGI, enviscope GmbH, Germany) and can be operated with either a backward or forward facing inlet geometry to sample the gas phase only or the sum of gas phase and (evaporated) particles. In order to ensure a low residence time in the inlet line and thereby reduce inlet artifacts, a bypass flow of up to 30 slm is established using an IDP-3 scroll pump (Agilent Technologies, USA) (Fig. 2). The general flight setup of the mass spectrometer is described below following the gas flow from the inlet line through the pressure regulated ionization chamber to the vacuum chamber of the mass spectrometer. Details on the ion source and in-flight calibration techniques are presented separately in Sects. 3 and 4.

2.1 Inlet line

For the inlet line of AIMS-H₂O we use a Synflex composite tube (Data Sheet, www.goodrichsales.com/products/pdfs/1300.pdf) with an outer diameter of 1/2". The tube consists of an aluminum body with an inner ethylene copolymer film and an outer polyethylene jacket. The material combines several features which are of benefit for water vapor measurements in the aircraft. Adsorption of water vapor to the walls and diffusion through the walls of Synflex lines is comparable to stainless steel tubes. Furthermore, it is much more flexible than stainless steel tubing. An approximately 40 cm length of tube is fitted inside a HALO TGI and heated to 40 °C controlled by a bimetal switch. A 1.2 m length of tube is used to connect the TGI with the pressure regulation valve of AIMS-H₂O. Tubing connections are made using Swagelok stainless steel compression fittings. This part of the tubing is heated separately to 40 °C using a two-point temperature controller. Two tee fittings are integrated into the sample line as depicted in Fig. 2. The one directly at the TGI is used to add calibration gas and an optional dilution flow of dry synthetic air (Air Liquide GmbH, residual H₂O ~ 0.5 ppmv). The dilution flow can be added via a mass flow controller (Type 1179, MKS Instruments) allowing for dilution ratios up to 2 : 1. A third tee fitting allows subsampling of air into the instrument while the large inlet flow needed for measurements with high time resolution flows directly to the pump. Since the two configurations of AIMS require specific properties of the inlet line, two different tubing sets are installed in the aircraft: synflex and stainless steel for AIMS-H₂O and Fluoropolymers (PFA) for AIMS-TG.

2.2 Pressure regulation

In order to guarantee constant flow and pressure conditions in the ion source, flow reactor and mass spectrometer, we use an automatically controlled pressure regulation valve mounted upstream of the ion source (Fig. 2). For AIMS-H₂O, the ball valve consists of stainless steel with a modified PTFE (D1710 Type 1) sealing (Swagelok SS-42GS4). The pressure regulation has to be fast since it needs to compensate for

AMTD

8, 13525–13565, 2015

The airborne mass spectrometer AIMS – Part 1

S. Kaufmann et al.

Title Page

Abstract

Introduction

Conclusions

References

Tables

Figures



Back

Close

Full Screen / Esc

Printer-friendly Version

Interactive Discussion



The airborne mass spectrometer AIMS – Part 1

S. Kaufmann et al.

Title Page

Abstract

Introduction

Conclusions

References

Tables

Figures



Back

Close

Full Screen / Esc

Printer-friendly Version

Interactive Discussion



At high temperature, the CE of the catalyst only depends on the available reaction sites on the Pt mesh and the flow through the catalyst tube. With higher flow, the CE decreases since the mean residence time, and thus the potential available reaction time, is reduced. In order to increase the available reaction time, the MFC is located downstream of the catalyst tube as depicted in Fig. 3b so that the catalyst itself is exposed to a pressure of 2 bar. At flow rates below 60 sccm, the CE is 100 % within the uncertainties of H₂ mixing ratio, MFCs and the reference measurement. When increasing the flow up to the maximum of 500 sccm, the CE usually decreases down to around 60 %. This behavior is found to be stable over the typical timescale of airborne measurement campaigns of a few weeks. To assure a reproducible performance of the calibration source, it is regularly characterized by ground measurements using an MBW 373-LX dew point mirror (MBW Calibration AG, Switzerland) as reference instrument. Using the reference measurement the flow dependency of the CE can be approximated by a fit function. This enables the use of the complete range of gas flows through the catalyst and thus a range of the in-flight calibration from 0.5 up to 150 ppmv H₂O.

Over longer time spans, the CE can decrease significantly, strongly dependent on storage conditions, probably due to contamination of reaction sites on the Pt catalyst. Therefore, several treatments of the Pt mesh were tested in order to restore the reaction sites. We found, that a simple roughening of the Pt surface and thereby physically removing contaminated spots on the surface works best and can reliably restore optimal conversion conditions. However, the largest uncertainty in the calibration still arises from the stability of the H₂ to H₂O conversion on the catalyst. Including the uncertainty of the reference measurements (0.5 K in frost point according to manufacturer) and H₂O contamination in the H₂/zero air mixture (stable at less than 0.5 ppmv, including bottle to bottle differences), the total accuracy of the in-flight calibration source is around 6 %.

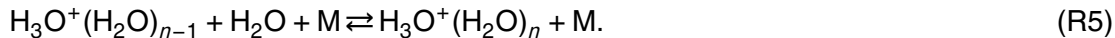
three-body-collision reaction



including either neutral nitrogen or oxygen molecules ($k = 2.6 \times 10^{-30} (T/300)^{3.2} \text{ cm}^6 \text{ s}^{-1}$, Payzant et al., 1973), ambient water vapor reacts with these educt ions to produce the primary product $\text{H}_3\text{O}^+(\text{H}_2\text{O})$ via the following reactions:



Reactions (R2)–(R4) have similar high rate constants on the order of $k = 1.5 \times 10^{-9} \text{ cm}^3 \text{ s}^{-1}$ and are thus very fast (Ferguson, 1974). For that reason a short distance between the ionization region and the entrance pinhole of the mass spectrometer is sufficient for the H_2O configuration. For the quantitative measurement of atmospheric water vapor we use $\text{H}_3\text{O}^+(\text{H}_2\text{O})$ as primary product ion at a mass-to-charge ratio of 37 amu (atomic mass unit). Since the reaction from H_2O to $\text{H}_3\text{O}^+(\text{H}_2\text{O})$ has multiple steps it cannot be considered as first order reaction. Thus the calibration of $\text{H}_3\text{O}^+(\text{H}_2\text{O})$ vs. H_2O is expected to be non-linear. Moreover, we also observe higher clusters of H_3O^+ with increasing H_2O formed by the reaction suggested by Cunningham et al. (1972):



In the upper troposphere and lower stratosphere, clusters with $n > 1$ do not contribute significantly to the H_3O^+ ion distribution. In more humid regions in the middle and lower troposphere, clusters with $n = 1$ to 3 show a significant signal. By using measurements of multiple clusters, AIMS- H_2O is able to measure water vapor from the lower troposphere up to the stratosphere.

The airborne mass spectrometer AIMS – Part 1

S. Kaufmann et al.

Title Page

Abstract

Introduction

Conclusions

References

Tables

Figures



Back

Close

Full Screen / Esc

Printer-friendly Version

Interactive Discussion



Apart from the H₂O branch of reactions described above, there are also multiple reaction pathways to form NO⁺ and NO₂⁺ ions from N₂⁺ and O₂⁺. Since nitrogen and oxygen are abundant in the atmosphere and no water vapor is included in these reactions, the signal of NO⁺ at $m/z = 30$ amu is used as an independent marker for the stability of the ionization and ion-molecule reaction process. The signal of NO₂⁺ is one order of magnitude lower than NO⁺ and exhibits a slight anticorrelation with H₂O.

4.3 Mass spectrum for the detection of water vapor

The reactions described above can be directly linked to the mass spectra measured with AIMS-H₂O. Four typical spectra corresponding to different water vapor mixing ratios are shown in Fig. 5. In the mass range shown, all ions have a single positive charge, hence the mass-to-charge ratio is identical to the ion mass. The H₃O⁺ ion at 19 amu exhibits a small positive correlation with H₂O, mainly due to fragmentation of H₃O⁺(H₂O) in the CDC. However, the overall signal is weak and not used for the evaluation of H₂O. NO⁺ exhibits a stable moderate signal at 30 amu and is independent of ambient water vapor. As expected from Reactions (R1) to (R4) the signal of O₂⁺ is very high at the lowest H₂O mixing ratios and anti-correlated with ambient water vapor since O₂⁺ represents the educt ion for the reaction with H₂O. Independent of the water vapor mixing ratio, we do not observe any significant signal on the intermediate ions from Reactions (R1) to (R4), namely O₄⁺ ($m/z = 64$), O₂⁺(H₂O) ($m/z = 50$) and H₃O⁺(OH) ($m/z = 36$). This suggests that the intermediate states are rather short-lived and the reaction path (R1–R4) already completed within the reaction chamber. As the reactions also suggest, the H₃O⁺(H₂O) ion at 37 amu shows the strongest correlation with water vapor and its signal strength is comparable to the O₂⁺ educt ion. Hence, the H₃O⁺(H₂O) signal can be used as direct measure for ambient water vapor mixing ratios. At H₂O mixing ratios above 500 ppmv, the higher cluster H₃O⁺(H₂O)₂ at 55 amu and H₃O⁺(H₂O)₃ at 73 amu become significant in terms of signal strength.

The airborne mass spectrometer AIMS – Part 1

S. Kaufmann et al.

Title Page

Abstract

Introduction

Conclusions

References

Tables

Figures



Back

Close

Full Screen / Esc

Printer-friendly Version

Interactive Discussion



5 Two data evaluation methods

The data reduction procedure begins with the evaluation of a laboratory or in-flight calibration and an appropriate application of the calibration to the flight data. In a second step, corrections for dilution, cross sensitivities or other influences on the measurement can be applied. For AIMS-H₂O we utilize two different methods to determine the atmospheric H₂O mixing ratio from the count rates measured by the mass spectrometer, both with benefits and disadvantages. Considering Reactions (R1) to (R4), a direct way to determine ambient H₂O is to calibrate the signal of the H₃O⁺(H₂O) on mass 37 amu at different water vapor mixing ratios. In doing so, one obtains a calibration as shown in Fig. 6b, derived from a typical calibration sequence (Fig. 6a). As expected from the multiple reaction steps to produce H₃O⁺(H₂O), the calibration function is non-linear. For water vapor mixing ratios below 30 ppmv, the number of H₂O molecules is the limiting factor. Since three water molecules are involved in the reaction pathway from O₂⁺ to H₃O⁺(H₂O), the calibration curve has a cubic shape in that region. For high H₂O, the available number of O₂⁺ educt ions becomes the limiting factor until at a certain H₂O mixing ratio all O₂⁺ ions are depleted by Reactions (R1) to (R4). Hence the cubic shape is expected to change into an exponential saturation. For H₂O mixing ratios > 500 ppmv in AIMS-H₂O, no new H₃O⁺(H₂O) ions are formed since O₂⁺ is completely depleted. However Reaction (R5) still alters the hydration of the existing ions towards higher clusters. In that region the amount of H₃O⁺(H₂O)₂ and H₃O⁺(H₂O)₃ increases at the expense of H₃O⁺(H₂O). Although the shape of the calibration curve can be well understood from the point of reaction kinetics, a fit with two different functions is rather impractical due to the high number of parameters and the uncertainty in the transition region. Therefore we apply a more pragmatic approach and use a logistic fit function:

$$y = \frac{A_1 - A_2}{1 + (x/x_0)^p} + A_2 \quad (1)$$

The airborne mass spectrometer AIMS – Part 1

S. Kaufmann et al.

Title Page

Abstract

Introduction

Conclusions

References

Tables

Figures



Back

Close

Full Screen / Esc

Printer-friendly Version

Interactive Discussion



6 Data quality and sources of uncertainty

The data quality depends on various factors with sensitivity of the instrument to a specific trace gas and signal noise being the most important ones. Additionally, any kind of drift effects modifying the count rates, cross sensitivities and uncertainties in the in-flight calibration change the data quality. In this work, we performed an extensive analysis of possible sources of uncertainty which is necessary to judge the reliability of the H₂O measurements in the atmosphere.

6.1 Sensitivity and detection limits

For the determination of signal noise, the in-flight calibration sequences are the most useful data since they are free of atmospheric variability and usually exhibit periods with stable signal long enough for sufficient statistics. The signal noise is best described by the standard deviation of the count rate, which increases with the absolute signal. Starting from an idealized statistical approach, the ion count rates can be described by a Poisson distribution. Hence, the standard deviation of the signal should equal the square root of the count rate. In reality, instrumental factors like variability of the discharge in the ion source, the transmission of the quadrupole and electrical noise from the detector increase the signal noise compared to the idealized value. For the complete AIMS setup, all these factors increase the signal noise roughly by a factor of two compared to pure statistical noise from Poisson theory.

However, data quality is not only determined by signal noise but equally by the instrument's sensitivity. For a linear calibration, sensitivity and signal noise are usually used to determine the detection limit (MacDougall and Crummett, 1980). The detection limit is the value below which the signal cannot be distinguished statistically from the background noise within a certain statistical significance. Assuming a constant calibration factor CF and a standard deviation σ_0 of the zero air signal, the detection limit DL is

The airborne mass spectrometer AIMS – Part 1

S. Kaufmann et al.

Title Page

Abstract

Introduction

Conclusions

References

Tables

Figures



Back

Close

Full Screen / Esc

Printer-friendly Version

Interactive Discussion



performed with AIMS-H₂O. In these calibrations, we did not observe any change in sensitivity of the H₃O⁺(H₂O) ion with or without additional CO₂.

7 Flight performance of AIMS-H₂O on HALO during ML-CIRRUS

AIMS-H₂O has been operated on the DLR Falcon in 2011 (Kaufmann et al., 2014; Voigt et al., 2014) and on HALO during the ML-CIRRUS experiment in March/April 2014. In order to provide an example of the performance of AIMS-H₂O, the water vapor time series of flight 9 on 7 April 2014 is shown in Fig. 8. The scope of this flight was to study contrail cirrus above Germany. The contrail cirrus were embedded in a frontal cirrus system extending above Western and Eastern Germany. In addition, we planned an intercomparison with ground based lidar measurements in Munich and Leipzig and with data from a radiosonde launched in Lindenberg. To this end, HALO took off from Oberpfaffenhofen, near Munich, at 7 UT and performed three transects in the heavily travelled airspace between Frankfurt and Berlin before returning to Oberpfaffenhofen. Two transects were selected for in situ measurements of contrail cirrus and natural cirrus while the third stratospheric transect focussed on remote sensing of the cirrus/contrail cirrus clouds with the onboard lidar system. Hence, in this flight we performed measurements inside cirrus clouds and in cloud free air at a range of water vapor mixing ratios down to 4 ppmv.

Besides data from AIMS-H₂O, H₂O mixing ratios measured by the tunable diode laser hygrometer SHARC are shown in Fig. 8. Both instruments measured gas phase water vapor via an actively pumped backward facing inlet. The agreement between the two instruments is excellent at water vapor mixing ratios below 150 ppmv during a large part of the flight after 36 000 s UTC. In particular, at H₂O mixing ratios down to 10 ppmv, the agreement is within $\pm 5\%$. Since the measurement range of the SHARC instrument is limited to mixing ratios above 10 ppmv, no comparison could be done for the flight legs in the lower stratosphere.

The airborne mass spectrometer AIMS – Part 1

S. Kaufmann et al.

Title Page

Abstract

Introduction

Conclusions

References

Tables

Figures



Back

Close

Full Screen / Esc

Printer-friendly Version

Interactive Discussion



The airborne mass spectrometer AIMS – Part 1

S. Kaufmann et al.

Title Page

Abstract

Introduction

Conclusions

References

Tables

Figures



Back

Close

Full Screen / Esc

Printer-friendly Version

Interactive Discussion



At the beginning of the flight between 33 300 and 35 600 s UT, H₂O mixing ratios measured by AIMS-H₂O were 12 to 15 % higher than the SHARC data, while short timescale H₂O variations were very similar. We speculate that AIMS-H₂O might overestimate the water vapor mixing ratio near 300 ppmv during that flight sequence due to a bias in the dilution correction. This effect is not permanent, but rather a feature observed only during that flight. However, the deviations are still within the combined uncertainty of both instruments. Regarding the relative humidity with respect to ice (RH_i) derived from H₂O mixing ratios and static air temperature measurements from HALO, AIMS measured slight mean supersaturation with respect to ice in that sequence while SHARC measured a slight mean subsaturation (lower panel in Fig. 9). Both instruments detected rapid fluctuations in RH_i between 60 and 140 %. Here we use the ice water content (IWC) calculated from total water vapor measurement by the WARAN tunable diode laser instrument as indicator for the occurrence of cirrus clouds (top panel in Fig. 9). The large variation in IWC suggests that we sampled a rather inhomogeneous cirrus cloud during the sequence from 33 300 to 35 600 s, which is consistent with the scatter of RH_i around saturation. In later parts of the measurement sequence in Fig. 9 (36 000 to 38 000 s), the IWC suggests a more dense and homogeneous cloud while both AIMS and SHARC indicate a mean subsaturation at around 91 %. For the two following cirrus penetrations at 37 000 and 37 800 s, RH_i is again fluctuating around saturation in both water vapor instruments.

In order to obtain a quantitative impression of the instrument performance over the entire campaign, Fig. 10 shows a scatter plot of H₂O mixing ratios measured by AIMS-H₂O and SHARC with an extensive set of 112 529 data points gathered in March/April 2014. The linear fit ($H_2O(\text{AIMS}) = 0.99961 \cdot H_2O(\text{SHARC}) + 0.01 \text{ ppmv}$) shows the excellent overall agreement between the instruments, with a very high correlation coefficient of 0.99568 giving high confidence in the data quality from both AIMS-H₂O and SHARC. The scatter of the data is comparable to the intercomparison published by Rollins et al. (2014).

While this paper focusses on the instrument description of AIMS-H₂O, a further detailed intercomparison of the set of water vapor instruments participating in ML-CIRRUS is out of the scope of this paper and will be published elsewhere.

8 Summary and outlook

5 With the airborne mass spectrometer AIMS, we developed a measurement technique to quantify low water vapor mixing ratios typical for the upper troposphere and lower stratosphere. To this end, we built a new gas discharge ion source which directly ionizes ambient air sucked in via a backward facing inlet. In a multi-step reaction similar to the reactions in the D-region of the ionosphere, water vapor molecules in ambient air
10 react to H₃O⁺(H₂O)_{*n*} (*n* = 0, . . . , 3) ions which are detected by the mass spectrometer. We perform a comprehensive and in-depth error analysis and achieve a high accuracy between 8 and 15 % in the measurement range between 1 and 500 ppmv, depending on specific humidity and time resolution of the measurement. The accuracy is estab-
15 lished by a regular in-flight calibration of the instrument using a water vapor standard generated by the catalytic reaction of hydrogen and oxygen on a heated Pt surface.

In order to increase the signal quality, two different data evaluation methods are used to determine ambient water vapor mixing ratios from the respective ion count rates. For water vapor mixing ratios below 15 ppmv we directly use the count rate of H₃O⁺(H₂O) at *m/z* = 37 to determine atmospheric water vapor. For higher mixing ratios, a normalized signal including all water vapor dependent ions provides a better data quality. Major
20 other contributors to uncertainty in the measurement are contamination of the vacuum chamber and inlet line with water vapor, and especially the temperature dependence of the quadrupole transmission.

AIMS-H₂O has been successfully deployed on the two DLR reserch aircraft Falcon
25 and HALO during CONCERT in 2011 and ML-CIRRUS in 2014, where the comparison with airborne TDL hygrometer SHARC showed a reasonable agreement within ±10 % for most of the data.

The airborne mass spectrometer AIMS – Part 1

S. Kaufmann et al.

Title Page

Abstract

Introduction

Conclusions

References

Tables

Figures



Back

Close

Full Screen / Esc

Printer-friendly Version

Interactive Discussion



References

- Chen, J.: Direct Current Corona-Enhanced Chemical Reactions, PhD Thesis, Department of Mechanical Engineering, University of Minnesota, 2002.
- Cunningham, A. J., Payzant, J. D., and Kebarle, P.: Kinetic study of the proton hydrate $H^+(H_2O)_n$ equilibria in the gas phase, *J. Am. Chem. Soc.*, 94, 7627–7632, doi:10.1021/ja00777a003, 1972.
- Dinh, T. and Fueglistaler, S.: Microphysical, radiative, and dynamical impacts of thin cirrus clouds on humidity in the tropical tropopause layer and lower stratosphere, *Geophys. Res. Lett.*, 41, 6949–6955, doi:10.1002/2014GL061289, 2014.
- Dinh, T., Fueglistaler, S., Durran, D., and Ackerman, T.: Cirrus and water vapour transport in the tropical tropopause layer – Part 2: Roles of ice nucleation and sedimentation, cloud dynamics, and moisture conditions, *Atmos. Chem. Phys.*, 14, 12225–12236, doi:10.5194/acp-14-12225-2014, 2014.
- Fahey, D. W., Gao, R.-S., Möhler, O., Saathoff, H., Schiller, C., Ebert, V., Krämer, M., Peter, T., Amarouche, N., Avallone, L. M., Bauer, R., Bozóki, Z., Christensen, L. E., Davis, S. M., Durre, G., Dyroff, C., Herman, R. L., Hunsmann, S., Khaykin, S. M., Mackrodt, P., Meyer, J., Smith, J. B., Spelten, N., Troy, R. F., Vömel, H., Wagner, S., and Wienhold, F. G.: The AquaVIT-1 intercomparison of atmospheric water vapor measurement techniques, *Atmos. Meas. Tech.*, 7, 3177–3213, doi:10.5194/amt-7-3177-2014, 2014.
- Fehsenfeld, F. C., Mosesman, M., and Ferguson, E. E.: Ion-molecule reactions in an $O_2^+-H_2O$ system, *J. Chem. Phys.*, 55, 2115–2120, doi:10.1063/1.1676382, 1971.
- Ferguson, E. E.: Laboratory measurements of ionospheric ion-molecule reaction rates, *Rev. Geophys. Space Phys.*, 12, 703–713, doi:10.1029/RG012i004p00703, 1974.
- Fite, W. L.: Positive ion reactions, *Can. J. Chem.*, 47, 1797–1807, doi:10.1139/v69-292, 1969.
- Forster, P. M. D. and Shine, K. P.: Assessing the climate impact of trends in stratospheric water vapor, *Geophys. Res. Lett.*, 29, 1086, doi:10.1029/2001gl013909, 2002.
- Gayet, J.-F., Shcherbakov, V., Voigt, C., Schumann, U., Schäuble, D., Jessberger, P., Petzold, A., Minikin, A., Schlager, H., Dubovik, O., and Lapyonok, T.: The evolution of microphysical and optical properties of an A380 contrail in the vortex phase, *Atmos. Chem. Phys.*, 12, 6629–6643, doi:10.5194/acp-12-6629-2012, 2012.

AMTD

8, 13525–13565, 2015

The airborne mass spectrometer AIMS – Part 1

S. Kaufmann et al.

Title Page

Abstract

Introduction

Conclusions

References

Tables

Figures



Back

Close

Full Screen / Esc

Printer-friendly Version

Interactive Discussion



The airborne mass spectrometer AIMS – Part 1

S. Kaufmann et al.

Title Page

Abstract

Introduction

Conclusions

References

Tables

Figures



Back

Close

Full Screen / Esc

Printer-friendly Version

Interactive Discussion



Groß, S., Wirth, M., Schäfler, A., Fix, A., Kaufmann, S., and Voigt, C.: Potential of airborne lidar measurements for cirrus cloud studies, *Atmos. Meas. Tech.*, 7, 2745–2755, doi:10.5194/amt-7-2745-2014, 2014.

Hansel, A., Jordan, A., Holzinger, R., Prazeller, P., Vogel, W., and Lindinger, W.: Proton transfer reaction mass spectrometry: on-line trace gas analysis at the ppb level, *Int. J. Mass Spectrom.*, 149–150, 609–619, doi:10.1016/0168-1176(95)04294-U, 1995.

Hegglin, M. I., Tegtmeier, S., Anderson, J., Froidevaux, L., Fuller, R., Funke, B., Jones, A., Lingenfeller, G., Lumpe, J., Pendlebury, D., Remsberg, E., Rozanov, A., Toohey, M., Urban, J., von Clarmann, T., Walker, K. A., Wang, R., and Weigel, K.: SPARC Data Initiative: comparison of water vapor climatologies from international satellite limb sounders, *J. Geophys. Res.*, 118, 11824–11846, doi:10.1002/jgrd.50752, 2013.

Hegglin, M. I., Plummer, D. A., Shepherd, T. G., Scinocca, J. F., Anderson, J., Froidevaux, L., Funke, B., Hurst, D., Rozanov, A., Urban, J., von Clarmann, T., Walker, K. A., Wang, H. J., Tegtmeier, S., and Weigel, K.: Vertical structure of stratospheric water vapour trends derived from merged satellite data, *Nat. Geosci.*, 7, 768–776, doi:10.1038/ngeo2236, 2014.

Heymsfield, A. J. and Miloshevich, L. M.: Relative humidity and temperature influences on cirrus formation and evolution: observations from wave clouds and FIRE II, *J. Atmos. Sci.*, 52, 4302–4326, doi:10.1175/1520-0469(1995)052<4302:rhratio>2.0.co;2, 1995.

Huey, L. G. and Lovejoy, E. R.: Reactions of SiF_5^- with atmospheric trace gases: ion chemistry for chemical ionization detection of HNO_3 in the troposphere, *Int. J. Mass. Spectrom.*, 155, 133–140, 1996.

Huey, L. G., Hanson, D. R., and Howard, C. J.: Reactions of SF_6^- and I^- with atmospheric trace gases, *J. Phys. Chem.*, 99, 5001–5008, doi:10.1021/j100014a021, 1995.

Hurst, D. F., Oltmans, S. J., Vomel, H., Rosenlof, K. H., Davis, S. M., Ray, E. A., Hall, E. G., and Jordan, A. F.: Stratospheric water vapor trends over Boulder, Colorado: analysis of the 30 year Boulder record, *J. Geophys. Res.*, 116, D02306, doi:10.1029/2010jd015065, 2011.

Jensen, E. J., Kinne, S., and Toon, O. B.: Tropical cirrus cloud radiative forcing – sensitivity studies, *Geophys. Res. Lett.*, 21, 2023–2026, doi:10.1029/94gl01358, 1994.

Jensen, E. J., Smith, J. B., Pfister, L., Pittman, J. V., Weinstock, E. M., Sayres, D. S., Herman, R. L., Troy, R. F., Rosenlof, K., Thompson, T. L., Fridlind, A. M., Hudson, P. K., Cziczo, D. J., Heymsfield, A. J., Schmitt, C., and Wilson, J. C.: Ice supersaturations exceeding 100 % at the cold tropical tropopause: implications for cirrus formation and dehydration, *Atmos. Chem. Phys.*, 5, 851–862, doi:10.5194/acp-5-851-2005, 2005.

The airborne mass spectrometer AIMS – Part 1

S. Kaufmann et al.

Title Page

Abstract

Introduction

Conclusions

References

Tables

Figures



Back

Close

Full Screen / Esc

Printer-friendly Version

Interactive Discussion



- Jeßberger, P., Voigt, C., Schumann, U., Sölch, I., Schlager, H., Kaufmann, S., Petzold, A., Schäuble, D., and Gayet, J.-F.: Aircraft type influence on contrail properties, *Atmos. Chem. Phys. Discuss.*, 13, 13915–13966, doi:10.5194/acpd-13-13915-2013, 2013.
- Jurkat, T., Voigt, C., Kaufmann, S., Zahn, A., Sprenger, M., Hoor, P., Bozem, H., Müller, S., Dörnbrack, A., Schlager, H., Bönisch, H., and Engel, A.: A quantitative analysis of stratospheric HCl, HNO₃, and O₃ in the tropopause region near the subtropical jet, *Geophys. Res. Lett.*, 41, 3315–3321, doi:10.1002/2013GL059159, 2014.
- Jurkat, T., Kaufmann, S., Voigt, C., Schäuble, D., Jeßberger, P., and Ziereis, H.: The airborne mass spectrometer AIMS – Part 2: Measurements of trace gases with stratospheric or tropospheric origin in the UTLS, *Atmos. Meas. Tech. Discuss.*, 8, 13567–13607, doi:10.5194/amtd-8-13567-2015, 2015.
- Kärcher, B., Dörnbrack, A., and Sölch, I.: Supersaturation variability and cirrus ice crystal size distributions, *J. Atmos. Sci.*, 71, 2905–2926, doi:10.1175/JAS-D-13-0404.1, 2014.
- Kaufmann, S., Voigt, C., Jeßberger, P., Jurkat, T., Schlager, H., Schwarzenboeck, A., Klingebiel, M., and Thornberry, T.: In situ measurements of ice saturation in young contrails, *Geophys. Res. Lett.*, 41, 702–709, doi:10.1002/2013GL058276, 2014.
- Kiehl, J. T. and Trenberth, K. E.: Earth's annual global mean energy budget, *B. Am. Meteorol. Soc.*, 78, 197–208, doi:10.1175/1520-0477(1997)078<0197:eagmeb>2.0.co;2, 1997.
- Krämer, M., Schiller, C., Afchine, A., Bauer, R., Gensch, I., Mangold, A., Schlicht, S., Spelten, N., Sitnikov, N., Borrmann, S., de Reus, M., and Spichtinger, P.: Ice supersaturations and cirrus cloud crystal numbers, *Atmos. Chem. Phys.*, 9, 3505–3522, doi:10.5194/acp-9-3505-2009, 2009.
- Kübbeler, M., Hildebrandt, M., Meyer, J., Schiller, C., Hamburger, Th., Jurkat, T., Minikin, A., Petzold, A., Rautenhaus, M., Schlager, H., Schumann, U., Voigt, C., Spichtinger, P., Gayet, J.-F., Gourbeyre, C., and Krämer, M.: Thin and subvisible cirrus and contrails in a subsaturated environment, *Atmos. Chem. Phys.*, 11, 5853–5865, doi:10.5194/acp-11-5853-2011, 2011.
- Kürten, A., Rondo, L., Ehrhart, S., and Curtius, J.: Performance of a corona ion source for measurement of sulfuric acid by chemical ionization mass spectrometry, *Atmos. Meas. Tech.*, 4, 437–443, doi:10.5194/amt-4-437-2011, 2011.
- Liou, K. N.: Influence of cirrus clouds on weather and climate processes – a global perspective, *Mon. Weather Rev.*, 114, 1167–1199, doi:10.1175/1520-0493(1986)114<1167:ioccow>2.0.co;2, 1986.

The airborne mass spectrometer AIMS – Part 1

S. Kaufmann et al.

Title Page

Abstract

Introduction

Conclusions

References

Tables

Figures



Back

Close

Full Screen / Esc

Printer-friendly Version

Interactive Discussion



- MacDougall, D. and Crummett, W. B.: Guidelines for data acquisition and data quality evaluation in environmental chemistry, *Anal. Chem.*, 52, 2242–2249, doi:10.1021/ac50064a004, 1980.
- Manabe, S. and Wetherald, R. T.: Thermal equilibrium of the atmosphere with a given distribution of relative humidity, *J. Atmos. Sci.*, 24, 241–259, doi:10.1175/1520-0469(1967)024<0241:teotaw>2.0.co;2, 1967.
- McCrumb, J. L. and Arnold, F.: High-sensitivity detection of negative ions in the stratosphere, *Nature*, 294, 136–139, 1981.
- Meyer, J., Rolf, C., Schiller, C., Rohs, S., Spelten, N., Afchine, A., Zöger, M., Sitnikov, N., Thornberry, T. D., Rollins, A. W., Bozóki, Z., Tátrai, D., Ebert, V., Kühnreich, B., Mackrodt, P., Möhler, O., Saathoff, H., Rosenlof, K. H., and Krämer, M.: Two decades of water vapor measurements with the FISH fluorescence hygrometer: a review, *Atmos. Chem. Phys.*, 15, 8521–8538, doi:10.5194/acp-15-8521-2015, 2015.
- Oltmans, S., Rosenlof, K., Michelsen, H., Nedoluha, G., Pan, L., Read, W., Remsberg, E., and Schiller, C.: SPARC Report No. 2: Upper Tropospheric and Stratospheric Water Vapour: Chapter 2, 2000.
- Payzant, J. D., Cunningham, A. J., and Kebarle, P.: Temperature dependence of the rate constants for the third order reactions: $O_2^+ + 2O_2 = O_4^+ + O_2$ and $O_4^+ + 2O_2 = O_6^+ + O_2$, *J. Chem. Phys.*, 59, 5615–5619, doi:10.1063/1.1679914, 1973.
- Ramanathan, V., Cess, R. D., Harrison, E. F., Minnis, P., Barkstrom, B. R., Ahmad, E., and Hartmann, D.: Cloud-radiative forcing and climate – results from the Earth Radiation Budget Experiment, *Science*, 243, 57–63, doi:10.1126/science.243.4887.57, 1989.
- Riese, M., Ploeger, F., Rap, A., Vogel, B., Konopka, P., Dameris, M., and Forster, P.: Impact of uncertainties in atmospheric mixing on simulated UTLS composition and related radiative effects, *J. Geophys. Res.*, 117, D16305, doi:10.1029/2012JD017751, 2012.
- Rollins, A. W., Thornberry, T. D., Gao, R.-S., Hall, B. D., and Fahey, D. W.: Catalytic oxidation of H_2 on platinum: a robust method for generating low mixing ratio H_2O standards, *Atmos. Meas. Tech.*, 4, 2059–2064, doi:10.5194/amt-4-2059-2011, 2011.
- Rollins, A. W., Thornberry, T. D., Gao, R. S., Smith, J. B., Sayres, D. S., Sargent, M. R., Schiller, C., Krämer, M., Spelten, N., Hurst, D. F., Jordan, A. F., Hall, E. G., Vömel, H., Diskin, G. S., Podolske, J. R., Christensen, L. E., Rosenlof, K. H., Jensen, E. J., and Fahey, D. W.: Evaluation of UT/LS hygrometer accuracy by intercomparison during the NASA MACPEX mission, *J. Geophys. Res.*, 119, 2013JD020817, doi:10.1002/2013JD020817, 2014.

The airborne mass spectrometer AIMS – Part 1

S. Kaufmann et al.

Title Page

Abstract

Introduction

Conclusions

References

Tables

Figures



Back

Close

Full Screen / Esc

Printer-friendly Version

Interactive Discussion



Sassen, K. and Comstock, J. M.: A midlatitude cirrus cloud climatology from the facility for atmospheric remote sensing – Part III: Radiative properties, *J. Atmos. Sci.*, 58, 2113–2127, doi:10.1175/1520-0469(2001)058<2113:amcccf >2.0.co;2, 2001.

Schumann, U., Jeßberger, P., and Voigt, C.: Contrail ice particles in aircraft wakes and their climatic importance, *Geophys. Res. Lett.*, 40, 2867–2872, doi:10.1002/grl.50539, 2013.

Solomon, S., Rosenlof, K. H., Portmann, R. W., Daniel, J. S., Davis, S. M., Sanford, T. J., and Plattner, G. K.: Contributions of stratospheric water vapor to decadal changes in the rate of global warming, *Science*, 327, 1219–1223, doi:10.1126/science.1182488, 2010.

Thornberry, T. D., Rollins, A. W., Gao, R. S., Watts, L. A., Ciciora, S. J., McLaughlin, R. J., Voigt, C., Hall, B., and Fahey, D. W.: Measurement of low-ppm mixing ratios of water vapor in the upper troposphere and lower stratosphere using chemical ionization mass spectrometry, *Atmos. Meas. Tech.*, 6, 1461–1475, doi:10.5194/amt-6-1461-2013, 2013.

Viggiano, A. A.: In situ mass spectrometry and ion chemistry in the stratosphere and troposphere, *Mass Spectrom. Rev.*, 12, 115–137, doi:10.1002/mas.1280120203, 1993.

Voigt, C., Schumann, U., Jurkat, T., Schäuble, D., Schlager, H., Petzold, A., Gayet, J.-F., Krämer, M., Schneider, J., Borrmann, S., Schmale, J., Jessberger, P., Hamburger, T., Lichtenstern, M., Scheibe, M., Gourbeyre, C., Meyer, J., Kübbeler, M., Frey, W., Kalesse, H., Butler, T., Lawrence, M. G., Holzäpfel, F., Arnold, F., Wendisch, M., Döpelheuer, A., Gottschaldt, K., Baumann, R., Zöger, M., Sölch, I., Rautenhaus, M., and Dörnbrack, A.: In-situ observations of young contrails – overview and selected results from the CONCERT campaign, *Atmos. Chem. Phys.*, 10, 9039–9056, doi:10.5194/acp-10-9039-2010, 2010.

Voigt, C., Schumann, U., Jessberger, P., Jurkat, T., Petzold, A., Gayet, J. F., Kramer, M., Thornberry, T., and Fahey, D. W.: Extinction and optical depth of contrails, *Geophys. Res. Lett.*, 38, L11806, doi:10.1029/2011gl047189, 2011.

Voigt, C., Jessberger, P., Jurkat, T., Kaufmann, S., Baumann, R., Schlager, H., Bobrowski, N., Giuffrida, G., and Salerno, G.: Evolution of CO₂, SO₂, HCl, and HNO₃ in the volcanic plumes from Etna, *Geophys. Res. Lett.*, 41, 2196–2203, doi:10.1002/2013GL058974, 2014.

Vömel, H., David, D. E., and Smith, K.: Accuracy of tropospheric and stratospheric water vapor measurements by the cryogenic frost point hygrometer: instrumental details and observations, *J. Geophys. Res.*, 112, D08305, doi:10.1029/2006jd007224, 2007.

Weinstock, E. M., Smith, J. B., Sayres, D. S., Pittman, J. V., Spackman, J. R., Hints, E. J., Hanisco, T. F., Moyer, E. J., St Clair, J. M., Sargent, M. R., and Anderson, J. G.: Validation of the Harvard Lyman-alpha in situ water vapor instrument: implications for the

mechanisms that control stratospheric water vapor, J. Geophys. Res., 114, D23301, doi:10.1029/2009jd012427, 2009.

Discussion Paper | Discussion Paper | Discussion Paper | Discussion Paper | Discussion Paper

AMTD

8, 13525–13565, 2015

The airborne mass spectrometer AIMS – Part 1

S. Kaufmann et al.

Title Page

Abstract

Introduction

Conclusions

References

Tables

Figures



Back

Close

Full Screen / Esc

Printer-friendly Version

Interactive Discussion



The airborne mass spectrometer AIMS – Part 1

S. Kaufmann et al.

Title Page

Abstract

Introduction

Conclusions

References

Tables

Figures



Back

Close

Full Screen / Esc

Printer-friendly Version

Interactive Discussion



Table 1. Measurement range, accuracy and precision for AIMS-H₂O. Remarks concern the parameters used to determine the precision and detection limit. For AIMS-H₂O, the two values for precision correspond to the two evaluation schemes using ion mass 37 amu (H₃O⁺(H₂O)) and ion ratio, respectively.

	Sensitivity (counts ppmv ⁻¹)	Accuracy (%)	Precision (%)		Remark
			37 amu	ir	
Global (1–500 ppmv)	50–400	7–15	4–15	1.5–15	Precision for 4 Hz data
@ 5 ppmv (stratospheric)	180	7	10 (7)	15 (8)	Precision for both evaluation methods and 4 Hz (1 Hz) data
@ 100 ppmv (tropospheric)	400	11	6.5 (4.5)	2 (1.7)	Same as above with 1 : 1 dilution ratio



Figure 1. Front view of instrument rack in AIMS-H₂O configuration integrated in a HALO standard rack. The inlet line is connected to a trace gas inlet (TGI) mounted at the top fuselage of the aircraft.

AMTD

8, 13525–13565, 2015

The airborne mass spectrometer AIMS – Part 1

S. Kaufmann et al.

Title Page

Abstract

Introduction

Conclusions

References

Tables

Figures

◀

▶

◀

▶

Back

Close

Full Screen / Esc

Printer-friendly Version

Interactive Discussion



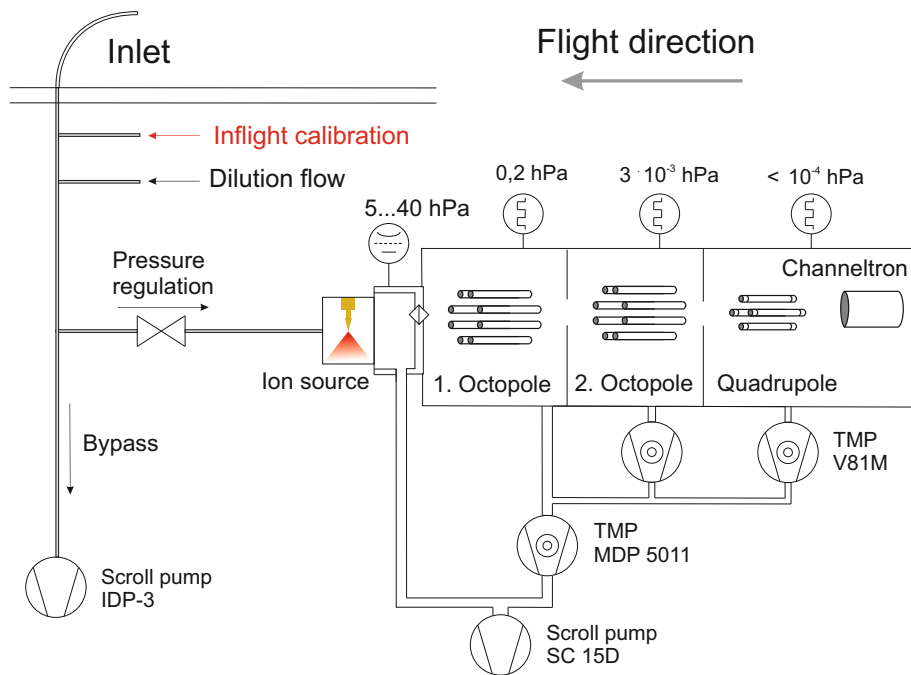


Figure 2. Schematic of the flight configuration of AIMS. Ambient air enters via a backward faced inlet and passes a pressure regulation valve before entering the ion source. The detailed setup of the ion source for the two measurement modes is depicted in Fig. 4. The ion beam is then focussed by two adjacent octopoles and finally separated by mass-to-charge ratio in the quadrupole. Additionally, connections for an optional dilution of ambient air and background measurements and for addition of trace gases for in-flight calibration (detail in Fig. 3) are mounted right beneath the inlet.

The airborne mass spectrometer AIMS – Part 1

S. Kaufmann et al.

Title Page	
Abstract	Introduction
Conclusions	References
Tables	Figures
◀	▶
◀	▶
Back	Close
Full Screen / Esc	
Printer-friendly Version	
Interactive Discussion	



The airborne mass spectrometer AIMS – Part 1

S. Kaufmann et al.

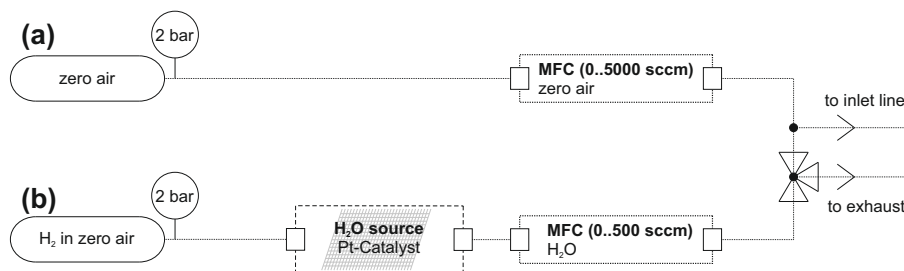


Figure 3. Setup of the in-flight calibration: **(a)** zero air can be added to the sample flow for dilution and background measurements. **(b)** A mixture of H₂ in zero air is passed over a heated Pt-catalyst and reacts to H₂O for calibration of the water vapor configuration. The water vapor mixing ratio in the calibration gas can be further adjusted by dilution with synthetic air from **(a)**. To allow for equilibration of the catalytic source, the calibration gas flow is switched on early and guided to the exhaust line before starting a calibration sequence.

Title Page

Abstract

Introduction

Conclusions

References

Tables

Figures

◀

▶

◀

▶

Back

Close

Full Screen / Esc

Printer-friendly Version

Interactive Discussion



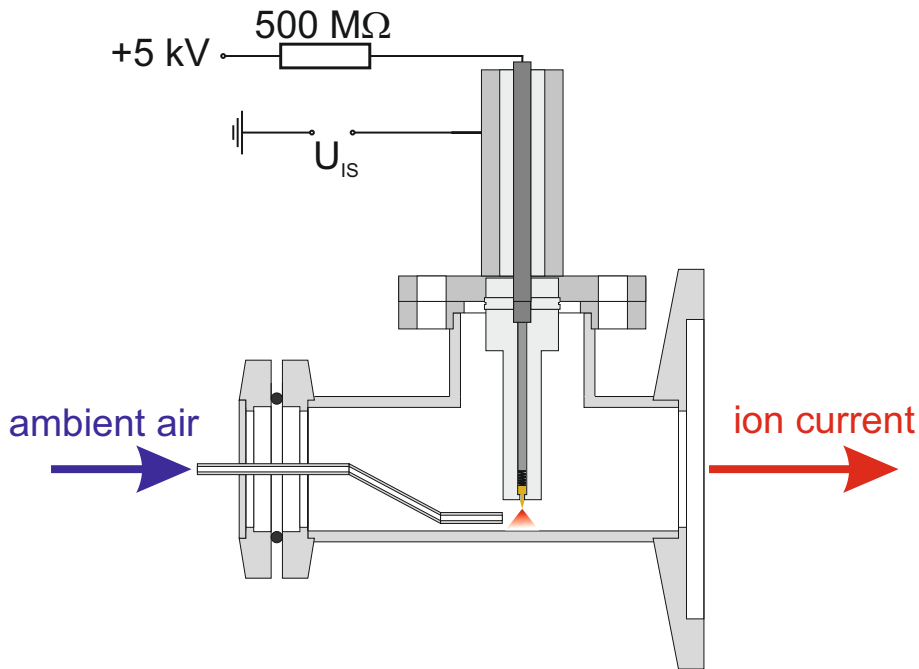


Figure 4. Gas discharge ion source of AIMS-H₂O: ambient air is guided to the discharge zone between a gold needle and the wall of the source (red shaded region). The needle has a positive potential of +5 kV relative to the shielding of the assembly which itself can be set at variable potential vs. ground. The resistance of 500 MOhm ist integrated in order to limit the maximum ion current to 0.01 mA.

The airborne mass spectrometer AIMS – Part 1

S. Kaufmann et al.

Title Page	
Abstract	Introduction
Conclusions	References
Tables	Figures
◀	▶
◀	▶
Back	Close
Full Screen / Esc	
Printer-friendly Version	
Interactive Discussion	



The airborne mass spectrometer AIMS – Part 1

S. Kaufmann et al.

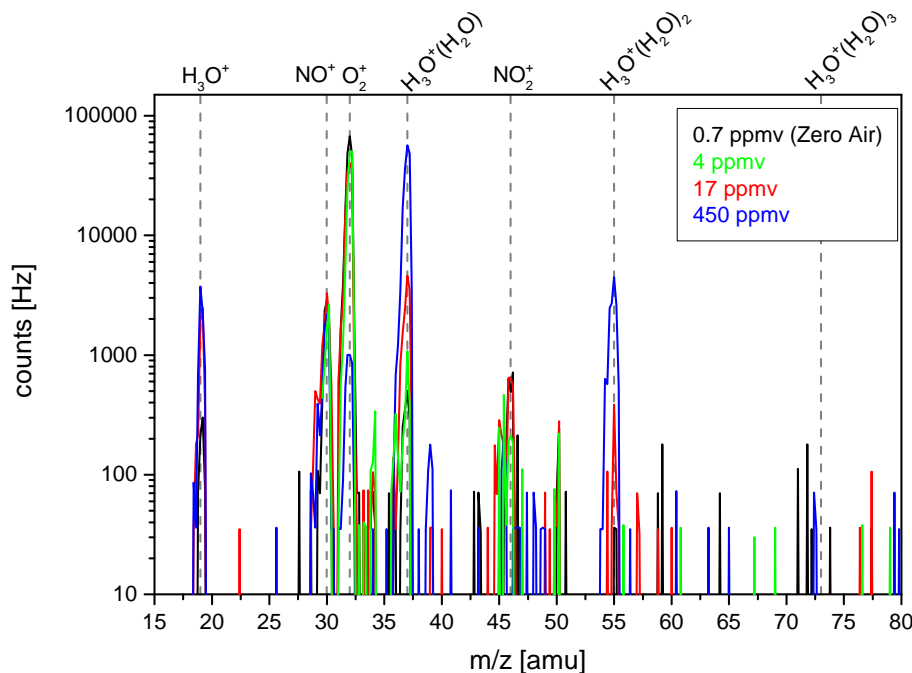


Figure 5. Mass spectra for m/z ratios from 15 to 80 amu for four different water vapor mixing ratios. The black curve represents a measurement of an added zero air flow, the other three spectra are samples of ambient atmospheric air during flight. As H_2O mixing ratios increase, the signals on H_3O^+ , $\text{H}_3\text{O}^+(\text{H}_2\text{O})$ and (@450 ppmv) $\text{H}_3\text{O}^+(\text{H}_2\text{O})_2$ increase whereas the O_2^+ signal decreases. The signal on $\text{H}_3\text{O}^+(\text{H}_2\text{O})_3$ does not increase up to mixing ratios of 450 ppmv. NO^+ and NO_2^+ stay almost constant over the range of water vapor mixing ratios shown here.

The airborne mass spectrometer AIMS – Part 1

S. Kaufmann et al.

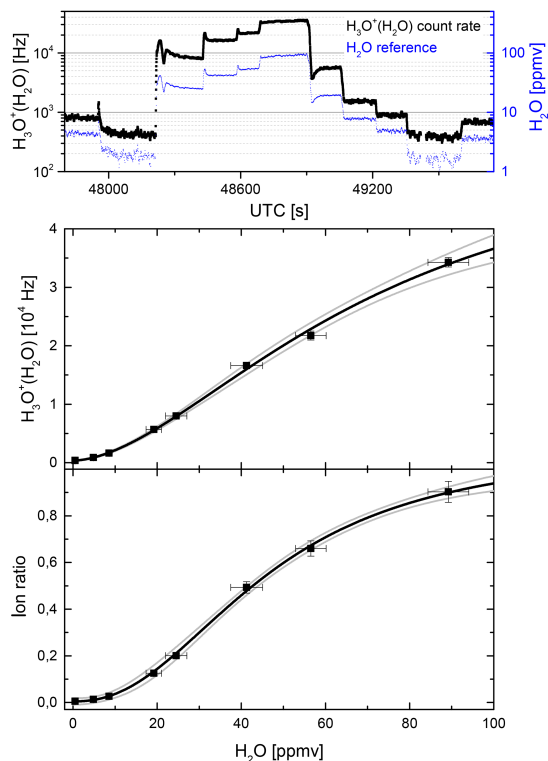


Figure 6. In-flight calibration curves for two different evaluation methods. Top: Time series of the $\text{H}_3\text{O}^+(\text{H}_2\text{O})$ ($m/z = 37$ amu) signal (black) and the corresponding water vapor mixing ratio (blue) for a characteristic calibration sequence. Middle: Count rate on $m/z = 37$ amu vs. H_2O in the calibration gas. In the lower panel the ratio of ion masses $(19+37+55)/(19+32+37+46+55)$ is plotted against H_2O . The grey curves mark the 95 % confidence interval of the respective fit curves.

The airborne mass spectrometer AIMS – Part 1

S. Kaufmann et al.

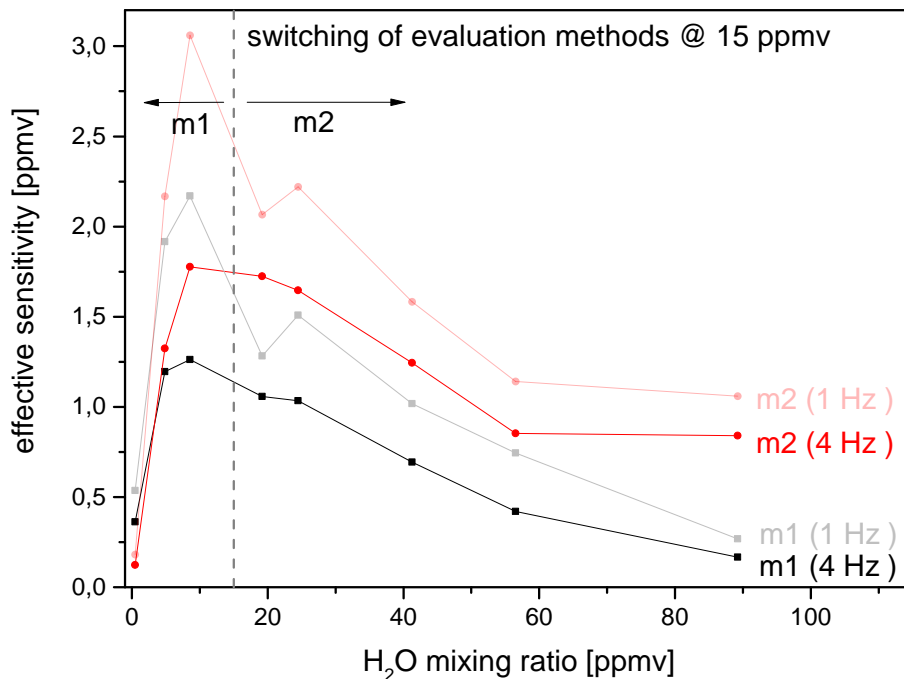


Figure 7. Effective sensitivity (as defined in Eq. 9) for evaluation method 1 (black) and method 2 (red). ES increases up to ~ 10 ppmv due to the increase in the slope of the calibration curve. At higher mixing ratios, the decrease of ES is caused by increasing signal noise. Below 15 ppmv, method 1 is used for calculation of atmospheric mixing ratios, above 15 ppmv, method 2 is used.

The airborne mass spectrometer AIMS – Part 1

S. Kaufmann et al.

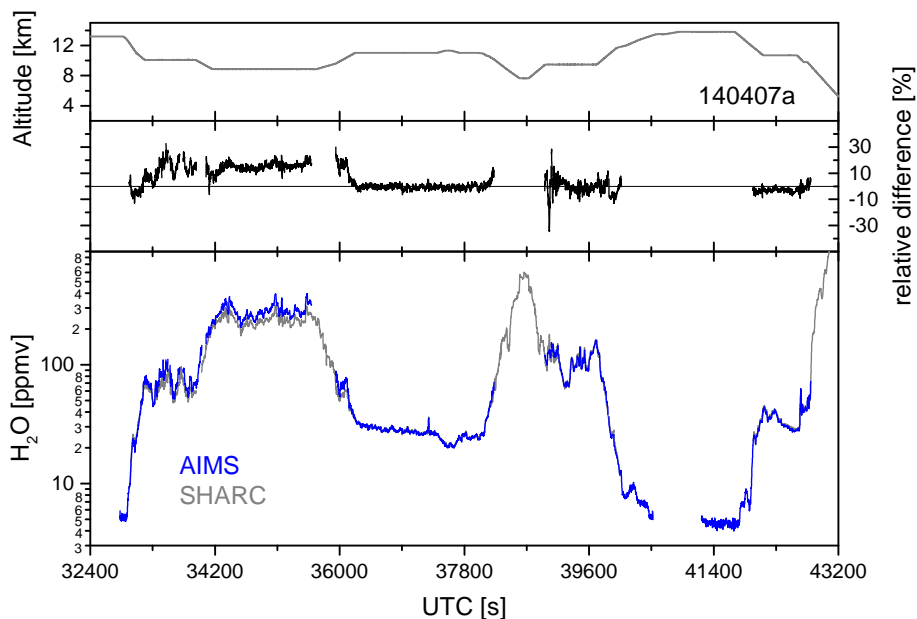


Figure 8. Time series of H_2O mixing ratio (bottom panel) from a flight on 7 April 2015 during the ML-CIRRUS campaign. The blue curve is the gas phase measurement of AIMS- H_2O . For comparison, measured mixing ratios from the SHARC TDL (grey) are shown. The top panel shows the flight altitude, the middle panel denotes the relative difference between both instruments. Data from both instruments agree reasonably well.

[Title Page](#)[Abstract](#)[Introduction](#)[Conclusions](#)[References](#)[Tables](#)[Figures](#)[◀](#)[▶](#)[◀](#)[▶](#)[Back](#)[Close](#)[Full Screen / Esc](#)[Printer-friendly Version](#)[Interactive Discussion](#)

The airborne mass spectrometer AIMS – Part 1

S. Kaufmann et al.

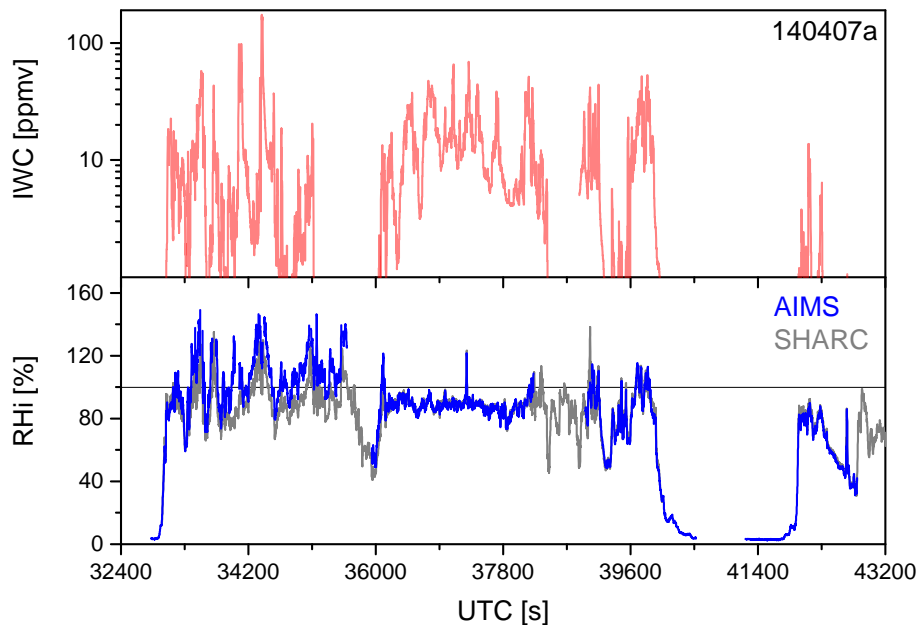


Figure 9. Top: ice water content (IWC) as cloud marker derived from total water measurements by the WARAN tunable diode laser instrument. Bottom: relative humidity with respect to ice calculated from AIMS H₂O mixing ratios (blue curve) and SHARC mixing ratios (grey curve) using the HALO static air temperature measurement. Except for the middle part from 36 000 to 38 000 s where the in-cloud RH_i is consequently below 100 %, RH_i typically scatters around saturation inside the clouds.

[Title Page](#)[Abstract](#)[Introduction](#)[Conclusions](#)[References](#)[Tables](#)[Figures](#)[◀](#)[▶](#)[◀](#)[▶](#)[Back](#)[Close](#)[Full Screen / Esc](#)[Printer-friendly Version](#)[Interactive Discussion](#)

